LIMNOLOGY and OCEANOGRAPHY

ASLO

Limnol. Oceanogr. 9999, 2024, 1–14

doi: 10.1002/lno.12486

Monitoring ecological dynamics on complex hydrothermal structures: A novel photogrammetry approach reveals fine-scale variability of vent assemblages

Loïc Van Audenhaege,[1,2*] **Jozée Sarrazin**,[1] **Pierre Legendre**,[3] **Garance Perrois**,[1,4] **Mathilde Cannat**,[5] **Aurélien Arnaubec**,[6] **Marjolaine Matabos**[1]

[1]Univ Brest, CNRS, Ifremer, UMR 6197 BEEP, Plouzané, France
[2]Ocean Biogeosciences, National Oceanography Centre, European Way, Southampton, UK
[3]Département de Sciences Biologiques, Université de Montréal, Montréal, Québec, Canada
[4]Tropical & Subtropical Research Center, Korea Institute of Ocean Science & Technology, Jeju, Republic of Korea
[5]Université Paris Cité, UMR 7154, CNRS et Institut de Physique du Globe de Paris, France
[6]Ifremer, Ctr Méditerranée, Unité Systèmes Marins, France

Abstract

We set out to characterize the fine-scale processes acting on interannual dynamics of deep-sea vent fauna by using a novel approach involving a 5-yr time series of 3D photogrammetry models acquired at the Eiffel Tower sulfide edifice (Lucky Strike vent field, Mid-Atlantic Ridge). Consistently, with the overall stability of the vent edifice, total mussel cover did not undergo drastic changes, suggesting that they have been at a climax stage for at least 25 yr based on previous data. Successional patterns showed consistency over time, illustrating the dynamic equilibrium of the ecological system. In contrast, microbial mats significantly declined, possibly due to magmatic events. The remaining environmental variability consisted of decimeter-scale displacement of vent outflows, resulting from their opening or closure or from the progressive accretion of sulfide material. As a result, vent mussels showed submeter variability in the immediate vicinity of vent exits, possibly by repositioning in response to that fine-scale regime of change. As former studies were not able to quantify processes at submeter scales in complex settings, this pioneering work demonstrates the potential of 3D photogrammetry models for conducting long-term monitoring in the deep sea. We observed that the ability of mussels to displace may enable them to cope with changing local conditions in a stable system. However, the long-term stability of mussel assemblages questions their capacity to withstand large-scale disturbances and may imply a low resilience of these "climax" communities. This suggests that they may be particularly vulnerable to the negative effects of mining activities in hydrothermal ecosystems.

Following the growing interest in seafloor massive sulfide deposits found at hydrothermal vents, potential environmental impacts must be evaluated for conservation purposes (Boschen et al. 2013). The acquisition of ecological knowledge to explain and predict the behavior of ecological systems requires the identification of the patterns, scales, and forces driving variability observed in natural communities over space and time (Sousa 1984). Ultimately, the characterization of functional traits allowing species to cope with that variability to maintain their populations can be used as baseline information for conservation purposes (Van Dover 2014).

Hydrothermal vents are characterized by the emission of heated fluids at the seafloor in ridges or basins displaying tectonic and volcanic activity. Venting can occur in the form of focused black or white smokers or diffuse outflows, each exhibiting different temperatures and concentrations of reduced minerals. Fluid composition and strength of venting are strongly influenced by the geological nature of the sub-seafloor, the geodynamical context of the region, and the

*Correspondence: loicva@noc.ac.uk, loic.vanaudenhaege@gmail.com

Additional Supporting Information may be found in the online version of this article.

Author Contribution Statement: J.S. and M.M. conceived this study. J.S., M.M., M.C. and L.V.A. participated in the collection of video sequences. A.A. and M.M. developed the photogrammetry and annotation software. A.A., M.M. and L.V.A. performed photogrammetry reconstruction. L.V.A. performed image annotations for models of 2018 and 2020. G.P., P.L., M.C., J.S., M.M. and L.V.A. performed analyses. L.V.A. wrote the manuscript. All authors reviewed the manuscript.

trajectory of seawater within the oceanic crust, including chemical reactions and phase separation induced by magmatism as well as by the pathway of percolation and advection that influences mixing processes (Barreyre et al. 2014; Chavagnac et al. 2018). Vent ecosystems support lush endemic communities that feature low species diversity and exceptionally high biomass that thrive despite the harshness of environmental conditions (Tunnicliffe 1991). Vent communities rely on chemoautotrophic microorganisms that harness energy from the oxidation of chemical compounds (H_2S, CH_4, Fe, and H_2) contained in the fluids, a process called chemosynthesis (Jannasch 1985). The vent habitat is highly heterogeneous, offering a variety of small-scale niches created by the vent fluid dilution gradient (Podowski et al. 2009; Lee et al. 2015). Species distributions are mainly driven by their physiological tolerance, nutritional needs, and biotic interactions (Mullineaux et al. 2003; Henry et al. 2008; Podowski et al. 2009).

In addition to this spatial heterogeneity, temporal dynamics interplay and contribute to the observed variability in ecosystems in general (Sousa 1984; Levin 1992). At vents, temporal variations and successions are typically monitored following interannual photographic transects to map megafaunal assemblages over time while avoiding the destructive effect of dredge or grab sampling (Sarrazin et al. 1997; Cuvelier et al. 2012). At intermediate to fast-spreading mid-ocean ridges (> 50–140 mm yr^{-1}), monitoring studies have usually started from a reference time after a broad-scale disturbance event (e.g., volcanic eruption) resetting communities to an early stage of colonization (Shank et al. 1998). In the absence of massive disturbance on ultra-slow to slow-spreading ridges (< 20–50 mm yr^{-1}), temporal series of images have underlined the small spatial scales (i.e., meter to submeter) at which interannual variability of faunal assemblages occurs on sulfide edifices (Copley et al. 2007; Sen et al. 2014; Du Preez and Fisher 2018).

However, for structures with complex topography, the detection of small-scale changes based on the analysis of two-dimensional (2D) images could be highly biased from a 3D perspective because of the resulting decrease in the accuracy of cover annotations, and the lack of precision of space–time observation tracking. Our ability to detect and explain fine-scale changes all warrant the use of 3D representations (Sarrazin and Juniper 1998). Structure-from-motion photogrammetry (Moulon et al. 2017) is an imaging technique used to build centimeter-scale resolution 3D mesh and textured models from 2D images acquired with a standard camera mounted on an underwater vehicle (Kwasnitschka et al. 2013). As structure-from-motion has become increasingly used for the past decade for underwater ecology (Pulido Mantas et al. 2023), it is employed for high-resolution mapping of deep-sea communities in complex topographical settings, including vent edifices and vertical walls (Gerdes et al. 2019; Robert et al. 2020). Since photogrammetry surveys have been successful at monitoring centimeter-scale changes in terrestrial and marine environments (D'Urban Jackson et al. 2020), their application to long-term monitoring of deep-sea communities could help unravel fine-scale processes of variability still largely unexplored by 2D imagery and integrate them in a broader knowledge of landscape ecology (Paine and Levin 1981).

This work pioneers the use of time series of high-resolution 3D models to retrieve accurate quantitative measurements and integrate different scales of dynamics of a complex deep-sea environment, from the decimeters to hundreds of meter scales. More specifically, this study aims to assess and quantify the temporal dynamics of the vent fauna and habitat on a deep-sea sulfide edifice and to characterize the processes influencing faunal variability.

Materials and methods

Study site

Lucky Strike is a basalt-hosted hydrothermal vent field located south of the Azores Islands on the Mid-Atlantic Ridge (MAR; Fig. 1A; Humphris et al. 2002), where a deep-sea observatory (EMSO-Azores) has been deployed for over a decade. Since then, yearly maintenance cruises have provided additional time series data (Matabos et al. 2022). Lucky Strike hosts the Eiffel Tower in the South-East, a mature hydrothermal edifice of ~ 450 m^2 that comprises a central ~ 11-m-high sulfide tower harboring focused venting activity surrounded by a mix of sulfide deposits and a sulfide-indurated slab displaying numerous cracks and flanges (Fig. 1B; Girard et al. 2020).

The Eiffel Tower topography is complex, with 5-m-high bulbous mounds at the base of the main vertical tower and inactive chimney structures located in the NW periphery (Fig. 1B,C). The fauna is characterized by patchy assemblages of vent-endemic invertebrates occupying distinct habitats along the vent fluid dilution gradient. At the Eiffel Tower, assemblages of *Mirocaris fortunata* shrimps and *Peltospira smaragdina* gastropods occupy the warmest habitats while colder areas host the symbiotic mussels *Bathymodiolus azoricus* dominating 90% of the biomass (Husson et al. 2017; Sarrazin et al. 2022). As exposure to the vent fluid declines with distance, the length of mussel individuals decreases, although their density and the richness of associated species increase (Sarrazin et al. 2020). Assemblages can be covered by white filamentous microbial mats dominated by sulfur-oxidizing *Beggiatoa* Gammaproteobacteria that benefit from the distal exposure to black smokers mediated by bottom currents and edifice topography (Crépeau et al. 2011; Girard et al. 2020). Dense aggregations of non-vent fauna and empty mussel shells are observed in the coldest habitats (Husson et al. 2017; Girard et al. 2020).

Temporal variability of Eiffel Tower vent communities has been studied over various scales. Previous work captured the impacts of infra-daily tidal modulation and biological interactions at the scale of a m^2 mussel assemblage (Matabos

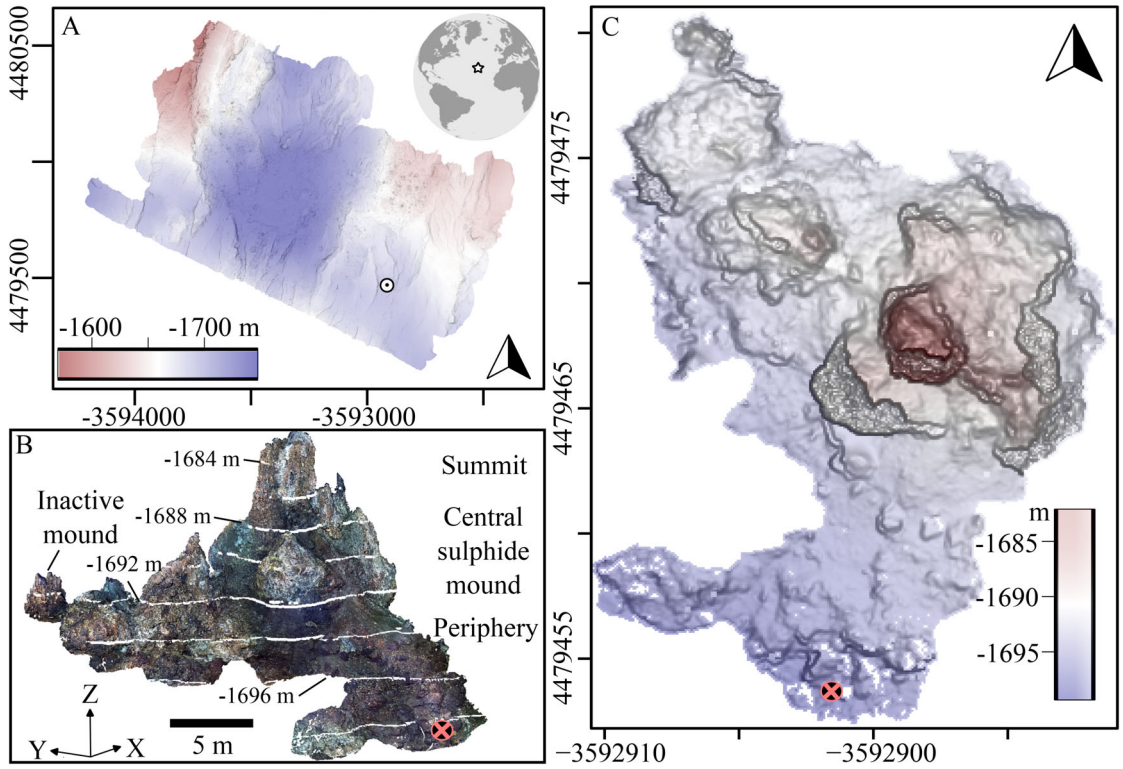

Fig. 1. (**A**) Bathymetric map of the Lucky Strike hydrothermal vent field (data from Ondréas et al. 2009). Upper left inset: the star designates the location of Lucky Strike in the Atlantic Ocean. The small circle indicates the Eiffel Tower hydrothermal edifice in Lucky Strike. Arrowhead indicates the north. (**B**) 3D textured model of the Eiffel Tower in 2015. The regions of the summit, central sulfide mound, periphery, and inactive mound in the North are indicated. Isobaths are delineated in white. (**C**) Downward-looking bathymetric map of the 3D model of Eiffel Tower in 2015. Arrowhead indicates the north. In panels (**B**) and (**C**), the red cross in a circle indicates the location of a vent assemblage monitored at sub-monthly time scales (Van Audenhaege et al. 2022).

et al. 2015; Mat et al. 2020), while remarkable stability was observed from monthly to 7-yr time windows (Cuvelier et al. 2017; Van Audenhaege et al. 2022). Pluriannual transects of 2D images from 1994 to 2008 suggested stability of the mussel assemblages at $\sim 100\ m^2$ over the edifice (Cuvelier et al. 2011*b*). Based on this work, we expect high temporal stability of vent faunal assemblages.

Building the dataset

Video sequences used for 3D reconstruction were acquired during three MoMARSAT cruises (Cannat and Sarradin 2010) by carrying out transects with a forward-looking camera mounted on the ROV *Victor6000* in April 2015 (HD videos for 4.33 h; Sarradin and Cannat 2015), August 2018 (HD videos for 5.23 h; Cannat 2018), and September 2020 (4K videos for 3.28 h; Sarradin and Legrand 2020). Lateral repetition of vertical video transects aimed to image all sides of the edifice from the summit to the base, by maintaining the ROV—insofar as possible—at a constant pace and distance from the edifice to produce overlap between vertical transects (i.e., at least 70% of image area). Images were extracted from video sequences every 3 s and color-corrected in the *Matisse* software (v.1.4.0; Arnaubec et al. 2023). These images were used to reconstruct three different textured 3D meshes of the Eiffel Tower for each survey year, using structure-from-motion techniques embedded in *Matisse*. The 3D reconstructions were georeferenced based on ROV navigation to provide (1) metric measurements of the surface and (2) spatial alignment (i.e., registration) among the 3D reconstructions. Since offsets sometimes larger than 1 m remained between georeferenced meshes, registration was performed by manual alignment of the models of 2018 and 2020 on the reconstruction of 2015 as reference. At least five corresponding points visibly stable through time were matched across models to compute the geometric transformation ("Align" tool of CloudCompare v.2.11). That task was performed on seven model portions of 2018 and 2020 cropped in "sides", as defined in the model of 2015 by Girard et al. (2020), originally to allow a smooth computer display. The final registration error among sides was assessed by generating 30 ground points equispaced by 4 m on the 2015 model ("Subsample" in CloudCompare). Close to each of the 30 points, a stable seabed feature was annotated in all models to compute offsets as a proxy for the registration error (Cucchiaro et al. 2018).

Annotation of the 3D models

To assess habitat and community variability within Eiffel Tower, the position of three types of observations was recorded over time: (1) substratum and biological cover, (2) vent outflows, and (3) topographic changes. All annotations were performed on the 3D mesh following the interpretation of textures, color, and spatial arrangement by loading the three models simultaneously as layers in *3DMetrics* software (v.0.6.0; Arnaubec et al. 2023). ROV video sequences were used to confirm annotation.

Biological assemblages and substrata were annotated with polygons and defined based on existing catalogs already used for annotation of the 2015 model (catalog in Supporting Information Fig. S1; Girard et al. 2020). Substratum categories were interpreted from their color, ranging from "black material" (recent sulfide-bearing deposits) to "white material" (anhydrite [$CaSO_4$] and barite [$BaSO_4$] deposits) or brownish oxidized sulfide-bearing material (hereafter "bare substratum"). Biological assemblages included the symbiotic mussel *B. azoricus* classified as small (mean length ± SD: 1.1 ± 0.6 cm), medium (3.3 ± 1.5 cm), or large individuals (6.0 ± 1.4 cm), zoanthids and empty shells (Cuvelier et al. 2009; *see* Girard et al. 2020 for measurements of mussel size classes). No differentiation was made between microcarnivorous sponges (i.e., possibly *Asbestopluma* sp., Cladorhizidae) and arboramminid foraminifera (i.e., possibly *Luffammina atlantica*); they were annotated as erect white morphospecies (Desbruyères et al. 2006). The additional presence of microbial mats on top of the assemblage/substratum was labeled. Following this protocol, each polygon was labeled with the time series of assemblage/substratum that the polygon contained in the three models. Annotation of cover stopped when only stable bare substratum remained unannotated. Independent annotations of *M. fortunata* and *P. smaragdina* assemblages, and individuals of the crab *Segonzacia mesatlantica* were not included in analyses, because of shrimp and crab mobility and high infra-annual dynamics, and *P. smaragdina* low abundance (only one stable assemblage of 0.04 m^2). ROV-induced displacement (e.g., avoidance or thruster blowing) and imagery detection difficulties (i.e., low size, hiding in mussel assemblages) may also occur (Cuvelier et al. 2012).

Vent fluid outflows were classified based on plume geometry, intensity, and color observed in ROV video sequences. They were relocated on the 3D models as points for focused vents, if the fluid was released from a discrete vent orifice, as points for diffusion zones, if only shimmering water was observed, and as lines in the case of flanges. Focused vents were sub-categorized based on the color of the venting fluid as (1) "black smoker" or (2) "white smoker."

Topographic changes were annotated as polygons after the detection of a modification in the mesh surface between 3D models. The process involved was specified from two main criteria: (1) if some material was lost or built up and (2) if the change involved material either exposed to venting and at least recently exposed (black or white material) or that remained inactive (bare substratum). In the case of flange accretion, the rate was determined from the average distance of flange progression, divided by the time separating both observations.

Polygon/point/line label, XYZ coordinates of the vertices and surface/length measured in the mesh were saved in *.json* files.

Data analyses

Dynamics of cover and succession among assemblages/substrata were monitored by quantifying the total cover through time as well as the amount of assemblage cover transiting from one to another over the edifice.

Spatial patterns of assemblage change were investigated by pooling polygons in tiles, as polygons are not a standardized surface of sampling. Permanent bare substratum and undetermined cover were excluded from pooling. The total surface of the polygons pooled in a tile could not exceed the largest polygon annotated (i.e., 2.4 m^2). The pooling was coded to account for spatial proximity among polygons; tiles, therefore, always formed continuous areas over space. Tiles covered 1.8 ± 0.4 m^2 (mean ± SD). Within a tile, a given polygon could only experience two types of dynamics: it remained unchanged (indicating "stability") or changed once (indicating "variability"). Those dynamics were computed by summing the surface of unchanged/changed polygons within a tile and for each assemblage. Tile variability can be further broken down as a combination of "net change" and "null change". The net change describes a local "gain" and/or "loss" of cover. The net change is obtained by subtracting the assemblage cover in 2015 from that of 2020 for each tile. The null change measures the surface of cover loss or gain of 2020 that was compensated by a cover gain or loss, respectively. The null change is measured by the difference between the total surface of change and the absolute value of the net change within a tile from 2015 to 2020. Those variables can be nested as circles of radius and width proportional to the area represented: the inner circle representing the net change, the inner torus representing the null change, and the outer one displaying unchanged cover. That symbology was plotted over space to assess patterns of stability and variability by locating tiles on the Eiffel Tower with their XYZ centroids.

Monitoring over 25 yr

To extend the monitoring up to 25 yr, we used 2D annotations obtained by Cuvelier et al. (2011*b*) on pluriannual photomosaics of the seven sides of the Eiffel Tower from 1994 to 2008. The surface of each 2D polygon (measured in pixels) was extracted from *.psd* annotation files in Python (v.3.7.4) and was summed by assemblage and substratum. Because covers were in pixels (1994–2008) and in square meters (2015–2020), they were standardized by dividing the cover annotated by the total surface annotated for each side of the

edifice to obtain proportional and relative covers. A univariate regression tree (URT) was applied to detect breakpoints in the time series of mussel and microbial mat covers, with the lowest possible relative error (RE) and cross-validated relative error (CVRE; Borcard et al. 2018).

Results

Registration accuracy

The distance among pairs of 3D models reached 0.06 ± 0.05 m (mean $\pm$ SD) and rarely exceeded 0.15 m (percentile 95% = 0.14 m).

Habitat changes

Changes in topography—rates of topographic change were 10.4 m^2 between 2015 and 2018 and 5.0 m^2 from 2018 to 2020. In total, this change accounted for only 4.4% of the surface annotated (Table 1). Over the whole time series, 77.9% of topographic change was related to active or recently active substratum. Overall, the majority of topographic change (77.3%) involved the building up of material; predominantly related to 107 hydrothermal features, either the directional growth of active geological features such as outcrops or flanges overhanging or blanketing the seabed (Table 1; Supporting Information Figs. S2–S4). Rate of flange accretion reached 0.05 ± 0.04 m yr^{-1} (mean $\pm$ SD) with a maximum value of 0.18 m yr^{-1} (Supporting Information Fig. S3). Voluminous changes at the base of large bulbous outcrops were related to the accretion of material in areas from which shimmering water was emitted (e.g., Supporting Information Fig. S5). Only vertical spires underwent repetitive growth and collapse (Table 1). Change in the inactive bare substratum was sporadic (Table 1) and was related to the fall of boulders from vertical faces (up to 0.8 m^2 for one observation).

Changes in the distribution of venting features—hydrothermal outflows concentrated within clusters of ~ 5 to ~ 30 m^2 that remained stable over time. Within those clusters, outflow distribution appeared to reposition over submeter scales (Fig. 2). In the South-East, we observed the activation of vent outflow with white material clearly emerging from a soft-sediment talus (Supporting Information Fig. S6).

Activity clusters consisted of a mix of diffusion zones, with white and black smokers often interspaced with flanges (Fig. 2). Counted black smokers were variable from 2015 ($n = 31$), 2018 ($n = 17$) to 2020 ($n = 39$). Overall, the number of white smokers doubled in 2015 ($n = 50$), stabilizing in 2018 ($n = 112$) and 2020 ($n = 119$). The number of flanges slightly increased from 70, 87, and 89 in 2020. Diffusion zones were stable from 2015 to 2018 ($n = 33$–37) and dropped dramatically in 2020 ($n = 17$).

Faunal and substratum dynamics

Total cover and successions among assemblages followed similar dynamics over time, between 2015 and 2018 and between 2018 and 2020, respectively (Supporting Information Fig. S7). As a result, we summarized them by summing flows of 2015–2018 and 2018–2020 together and by presenting the net change of total cover from 2015 to 2020 (Fig. 3).

Recently active substrata were predominantly represented by white material ($\sim 90\%$) that underwent a loss of 8.8 m^2 from 2015 to 2020. On average, the total area covered by all mussel assemblages increased from 254.7 m^2 in 2015 to 269.7 m^2 in 2020 to represent 59.7% of the total surface of the edifice (Fig. 3). The most abundant medium-mussel

Table 1. Characteristics of the topographic changes observed over 5 yr of monitoring at the Eiffel Tower hydrothermal edifice (total area imaged = 452 m^2). Net change is either positive (+; material accumulation) or negative (−; material loss) and involves (recently) active and inactive substrata. The surface that underwent change was computed using *3DMetrics* software, and the process and features involved were visually interpreted. The number of observations (*n*) is indicated in parentheses.

		Surface of change [m^2] (n = number of features)		
Net change	**Substratum characteristics**	**2015–2018**	**2018–2020**	**Process inferred from observations**
+	Active	0.4 (11)	0.4 (9)	Vertical accretion of spires
		4.0 (31)	3.4 (26)	Lateral/downward accretion of 3D outcrops
		1.6 (19)	0.7 (11)	Forward and downward accretion of linear features (flanges)
	Inactive	1.4 (19)	0.0 (0)	Debris build-up at the base of the edifice as scree or chimney fragments
	Total	**7.4 (80)**	**4.5 (46)**	
–	Active	0.9 (21)	0.4 (10)	Chimney collapse
		0.1 (1)	0.1 (2)	Outcrop detachment
	Inactive	2.0 (18)	0.0 (0)	Boulder detachment or scree displacement
	Total	**3.0 (40)**	**0.5 (12)**	

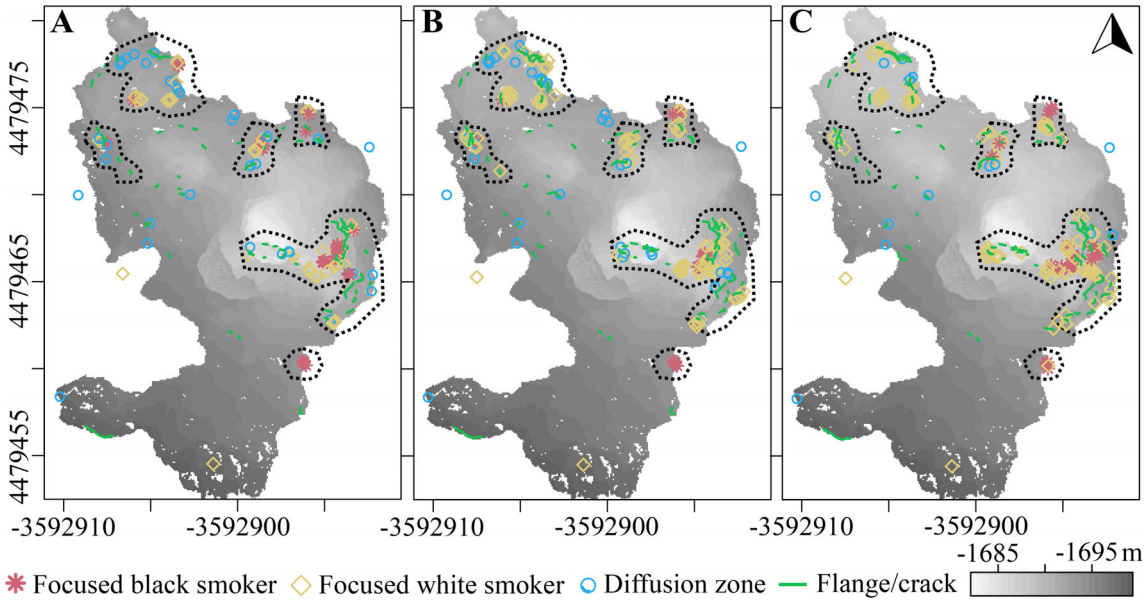

Fig. 2. Bathymetric maps positioning and describing the variability of venting features over the Eiffel Tower edifice in (**A**) 2015, (**B**) 2018, and (**C**) 2020. Black dotted polygons delimit hydrothermal areas harboring a continuous spatial aggregation of venting features identified based on ROV video sequences. Bathymetry is provided with a black-to-gray color gradient. Coordinates are in meters (EPSG: 3857). The arrowhead indicates the north.

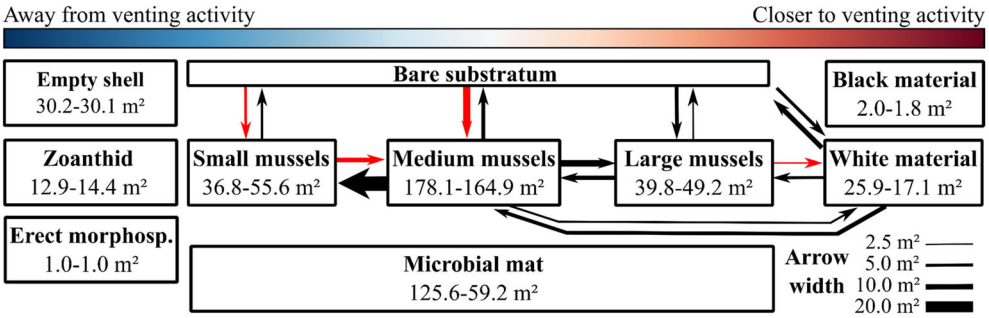

Fig. 3. Schematic summary of the successional model refined from Cuvelier et al. (2011*b*). Assemblages and substrata are ordered along their positions along the vent dilution gradient (*see* Cuvelier et al. 2009). Areas covered in 2015 and 2020 are displayed under the assemblage name. The arrow width in m^2 (scale on bottom right) and direction represent cover flows summed for 2015–2018 and 2018–2020. Red arrows highlight transfers also detected by Cuvelier et al. (2011*b*). Only flows > 1 m^2 are represented. *See* a higher level of detail in Supporting Information Fig. S7.

assemblages decreased slightly from 2015 to 2020 (−13.2 m^2), while the surface occupied by large- and small-mussel assemblages had gradually increased by 2020 of +9.4 and +18.8 m^2, respectively. In the periphery, zoanthids erected sessile species, and empty shells barely underwent any change over 5 yr. Microbial mat cover underwent a considerable cover loss of 52.9% from 2015 to 2020 (−66.4 m^2; Fig. 3).

The white material predominantly converted into bare substratum (8.9 m^2) or was colonized by large (5.3 m^2) and medium (6.8 m^2) mussels (Fig. 3). The white material also replaced the bare substratum (5.9 m^2), large (3.0 m^2), and medium (3.8 m^2) mussels. Colonization of mussels occurred on bare substratum (large: 6.9 m^2, medium: 13.2 m^2, small: 5.0 m^2). Large mussels were replaced by 8.0 m^2 of medium mussels, whereas 11.2 m^2 of medium individuals transitioned to larger ones (Fig. 3). Small-mussel assemblages transitioned to medium ones by 26.4 m^2 while 7.8 m^2 transited the opposite way. Large- and small-mussel assemblages rarely transitioned from one to the other directly (< 1.0 m^2) during the 5-yr time interval.

A substantial cover of mussel assemblages underwent a change from 2015 to 2020 for large—(54.6%), medium—(34.6%), and small—(59.2%; Fig. 4A–C). Cover of microbial mats displayed higher variability (71.3%; Fig. 4D).

Change in large- and medium-mussel assemblages occurred mostly within venting areas (Fig. 4A,B). Overall, changes consisted of a mix of anecdotic cover losses and gains interspaced with larger null changes within venting areas. Over the extent of the venting area, this pattern suggested the overall stability of the assemblages despite meter-scale changes. Still, a gain of large (+5.6 m^2) and medium mussels (+1.8 m^2) was detected

in the South-East venting area (Fig. 4a; Supporting Information Fig. S8, S9). Outside venting areas, where large mussels rarely occurred, medium-size mussels were stable, except for a large decrease in the center of the edifice (−11.0 m^2; Fig. 4B). That loss coincided with a gain of small mussels (+11.4 m^2; Fig. 4C). Overall, small mussels inhabiting areas outside direct venting gained cover over the edifice. That pattern coincided with the general loss of microbial mat cover (Fig. 4D). As for

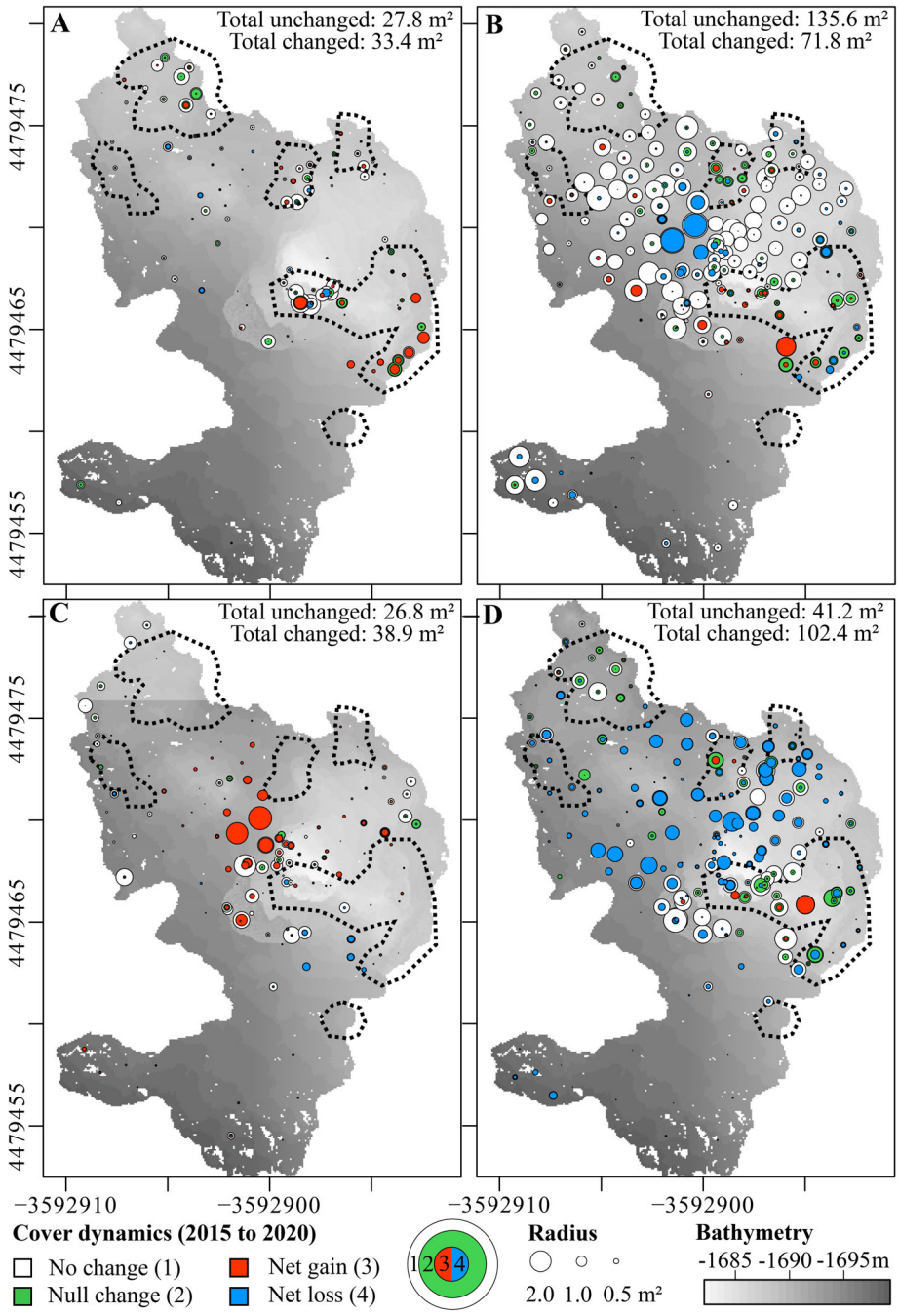

Fig. 4. Spatial distribution of assemblage cover dynamics of (**A**) large mussels, (**B**) medium mussels, (**C**) small mussels, and (**D**) microbial mats from 2015 to 2020. Each circle represents the dynamics occurring within a tile: (1) unchanged cover with the white outer torus, and cover that changed delimited by (2) null change with the green torus, and (3) gain or (4) loss with the red or blue inner circles, respectively. The radius/width of the circle/torus is proportional to the surface of the cover represented. The total surface of unchanged and changed cover from 2015 to 2020 combined is stated in the upper right inset corner. The total area of the edifice is 452 m^2. Black dotted polygons delimit areas harboring hydrothermal activity (*see* Fig. 2). Bathymetry is shown with a black-to-gray color gradient. Arrowheads indicate the north. Coordinates are in meters (EPSG: 3857).

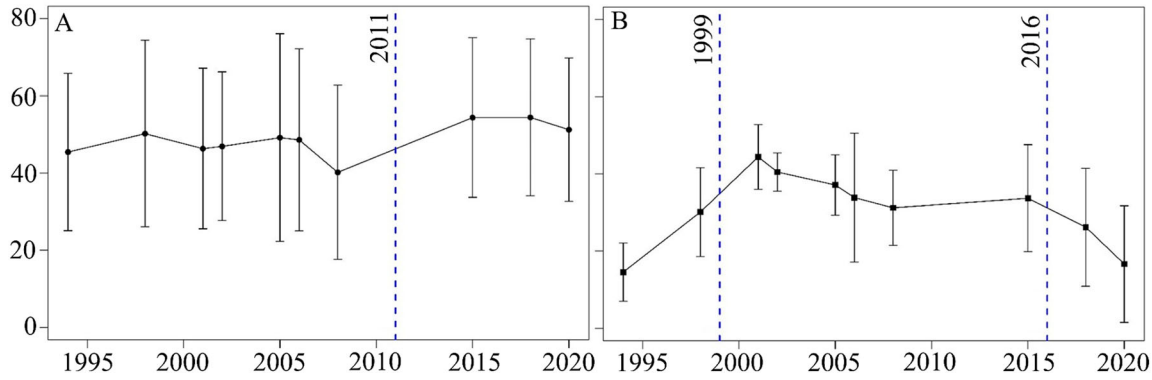

Fig. 5. Mean relative cover [%] of Eiffel Tower assemblages for (**A**) mussels (sum of small, medium, and large mussel covers) and (**B**) microbial mat cover. Dots represent the average assemblage cover computed between edifice sides for each time step from 1994 to 2008 (Cuvelier et al. 2011*b*) and from 2015 to 2020 (this study). Whiskers are the associated standard deviations of assemblage cover among sides. The blue dashed lines represent breaking points in the time series detected in the URT analysis.

large and medium mussels, microbial mats exhibited local patterns of variability, mostly within venting areas.

Over 25 yr, mussel total cover ranged from ~ 45% to 55% despite high variability among edifice sides (Fig. 5A). The URT analysis depicted a breakpoint between 2008 and 2015 (RE = 0.4, CVRE = 0.6). Microbial cover was less variable among edifice sides than for mussel cover, illustrating lower spatial heterogeneity of cover among sides (Fig. 5B). Microbial mat cover did not display a stable trend, ranging from ~ 15% to 45% on average over 25 yr (Fig. 5B). The URT identified breakpoints between 1998 and 2001 and between 2015 and 2018 (RE = 0.3, CVRE = 1.2). After an increase of ~ 30% of cover till 2001, microbial mat cover decreased by ~ 15% till it stabilized from 2008 to 2015. From 2015 to 2020, microbial mat cover declined by ~ 15% (Fig. 5B).

Discussion

Using a time series of 3D models, this study described the variability of hydrothermal vent assemblage cover through space and time and at different scales occurring over a complex deep-sea sulfide edifice. To our knowledge, this study is the first to apply 3D quantitative techniques to resolve the fine-scale dynamics of vent communities over 5 yr. It also extends the monitoring of the Eiffel Tower edifice up to 25 yr. This work establishes a methodological and analytical baseline workflow to disentangle variability from the broader 100-m^2 scale to the submeter scale, the latter having been rarely quantitatively investigated in the past (Cuvelier et al. 2011*b*; Sen et al. 2014).

Limitations

We estimated an average registration error among 3D models smaller than the decimeter, demonstrating the high spatiotemporal continuity of this study. Similar to registration error reported from terrestrial studies that used unmanned aerial vehicles (e.g., registration error ranging from 0.04 to 0.11 m in Cucchiaro et al. 2018), this result is a real achievement in a deep-sea context where the acquisition of imagery is constrained, not only by time but also by a number of technical challenges. For example, meter-scale drifts in ROV navigation among dives can increase registration errors. Visual relocation of the ROV based on the image time series could ultimately help improve the global registration of image, especially when considering the high stability of the Eiffel Tower edifice (Boittiaux et al. 2023).

Variability in image acquisition throughout years of sampling may also alter the accuracy of temporal monitoring, due to (1) variable distances of the ROV from the edifice across years, (2) differences in image sharpness due to changing turbidity or plume dispersion, and (3) change in camera resolution. This can ultimately lead to variability in photogrammetry model resolution and to difficulties in the identification of small organisms and vent outflows. The use of pre-programmed tracks and visual repositioning may be the only way to overcome sampling irregularities as it started to be implemented for the Eiffel Tower edifice (Boittiaux et al. 2023).

Habitat dynamics

Physical habitat—the Eiffel Tower has been a stable structure through time: less than 5% of the edifice surface underwent topographic modifications. Topographic changes occurred predominantly in areas restricted to the close vicinity of hydrothermal outflows due to the precipitation of minerals. The rapid formation of friable chimneys and spires, their collapse and accumulation on the soft-sediment talus, were only observed sporadically, likely because of their sub-monthly dynamics (Tunnicliffe and Juniper 1990; Van Audenhaege et al. 2022), which was not resolved in this case study. Those rapid dynamics at sub-monthly time scales, combined with the friability of spires and soft substratum of the talus, explain the scarcity of vent mussels in those areas that most likely rely

on a secured anchorage with their byssus threads to maintain themselves under appropriate vent exposure. Variability in the physical habitat occurred predominantly through outward accretion of hydrothermal features such as flanges and outcrops. As accretion proceeds at a rate of a dm yr^{-1} (Van Audenhaege et al. 2022; this study), the apparent switch from white material to consolidated and oxidized material suggests the build-up creation of vacant "bare substratum", as was also observed in Pacific vents (Du Preez and Fisher 2018). Since the observed collapse of oxidized material remained scarce, that bare substratum may persist for years. At larger decadal scales, the induration of newly formed vent material may contribute to the edifice build-up while supplying a solid hard substratum, opening habitats suitable for an effective attachment of vent organisms.

Hydrothermal activity—venting clustered in a few areas of several square meters, containing flanges, diffusion zones and focused emissions, and was mainly located on the sides of the mound. The stability of the location of those active clusters suggests the absence of major redistribution events of venting activity on and at the periphery of the structure (Sarrazin et al. 1997; Cuvelier et al. 2011*b*). Considering finer spatial scales, the repositioning of vent exits was predominantly restricted to changes within clusters. The mineral accretion and friable feature collapse, and the progressive subsurface clogging by mineral precipitates could explain submeter scale repositioning of vent fluid emission (Hannington et al. 1995; Sarrazin et al. 2002). Here, directional relocation of vent outflow predominated, following accretion and oxidation of hydrothermal material.

Faunal assemblage dynamics

Mussel dynamics—the megafaunal community was remarkably stable over time, consistent with the lack of dramatic changes in the hydrothermal and physical habitat, corroborating the high stability observed from 1994 to 2008 by Cuvelier et al. (2011*b*). It is generally assumed that randomness of biological change, as observed at vents in the East Pacific (Sarrazin et al. 1997), indicates a regime of chronic and patchy disturbance as proposed by Horn (1976) for plant communities. However, in the case of the Eiffel Tower, the consistency of an ordered succession model underlines the maintenance of spatial assemblage segregation as disturbances only occurred at small scales (Cuvelier et al. 2011*b*; this study). Despite that variability, the consistency of assemblage flow suggests an apparent "steady-state equilibrium" of the megafaunal community over the 5 yr of monitoring. In the absence of dramatic disturbance events (e.g., magmatic/tectonic disruption), an abundant mussel population (~ 263 m^2) has likely thrived there during at least three decades since the first scientific survey in 1992, supporting the hypothesis of a "climax" stage of a succession of Eiffel Tower communities (Cuvelier et al. 2011*b*).

The variability of large and medium mussels generally coincided with the meter-scale variability of vent fluid repositioning and topographic changes observed in venting areas of the Eiffel Tower. Other studies under continuous venting regimes have observed similar small-scale dynamics, as they remain inevitably the main drivers of natural variability in the absence of significant and large-scale habitat modifications (Copley et al. 2007; Sen et al. 2014; Du Preez and Fisher 2018). This confirms that the closer vent exits are to one another, the more dynamic the habitat will be and, consequently, the more vent megafaunal assemblages will likely vary. Small-scale change in the venting habitat is likely to trigger (1) a direct disturbance from material accretion or vent opening and (2) a change in conditions that will support or threaten organisms. Notwithstanding, mussels still displayed very low net change despite the high variability observed in the vicinity of vent exits, hence suggesting that any impact on mussel cover was compensated within 2–5 yr. This sustenance of populations over the venting habitat demonstrates that *B. azoricus* mussels have developed abilities to cope with small-scale changes in the vent habitat. The higher stability of medium mussel and zoanthid assemblages located away from the venting activity may be related to a more stable environment influenced by the cold deep-sea waters that dilute vent fluids and, therefore, buffer any distal influence of vent exposure change. In fact, *B. azoricus* may benefit from the edifice arrangement since the interaction of bottom currents with complex topography could provide a steady trophic supply by redistributing hydrothermal vent plume, preys, and suspended particles over a large area (Girard et al. 2020). However, a decrease in mussel sizes over the edifice summit may still be compatible with an overall slow decline of the Lucky Strike field activity, as proposed by Barreyre et al. (2012) based on a comparison of the 1996 and 2009 seafloor images. However, this pattern remains to be confirmed as the mussel population seemed relatively stable across 25 yr of monitoring despite a significant increase in mussel cover between 2008 and 2015. Although assemblage cover was standardized, that breakpoint remains difficult to confirm because of the methodological switch from opportunistic 2D data to more accurate 3D annotations.

Our characterization of the spatiotemporal scales of variability can help identify candidate traits contributing to the resilience of vent communities. In this study, we witnessed rates of flange accretion reaching < 0.1 m yr^{-1} (e.g., Supporting Information Fig. S2, S3) and (de)activation usually occurring within areas < 1 m^2 (e.g., Supporting Information Fig. S4). At infra-annual time scales, previous observation evidenced that, as accretion of new substratum proceeds, *B. azoricus* benefits from the indurated substratum to adapt their position to optimal vent fluid exposure through migration of large individuals (~ 0.1–0.3 m d^{-1}; Van Audenhaege et al. 2022) or, more slowly, of byssus-bounded aggregations (~ 0.1–0.2 m yr^{-1}; Van Audenhaege et al. 2022). As the migration capability of

B. azoricus is comparable to the scales of change we observed near vent outflows, it seems reasonable to state that mobility is a fundamental trait ensuring vent mussels cope with local habitat changes in active areas of the edifice, as previously hypothesized for vent mussels and gastropods of the Pacific Ocean (Johnson et al. 1994; Sen et al. 2014). On vent edifices, mobility and the ability to orientate migration may be particularly important to sustain a pole position in a habitat where small-scale changes are persisting, as also observed for Pacific vent gastropods (Sen et al. 2014). Taking advantage of these gradual small-scale changes could even help mussels rapidly gain access to vent exposure while avoiding the cost of intraspecific competition of dense aggregations (e.g., *see* Bertness and Grosholtz 1985). As dense assemblages of large mussels relocate, competition may be relaxed to allow the settlement of smaller mussels, for which recruitment was suggested to be inhibited by larviphagy, therefore resulting in size-based spatial segregation of mussels (Comtet and Desbruyères 1998; Lenihan et al. 2008). In the case of vent exposure increase, smaller mussels could still hold the capability to modify their endosymbiont community through environmental acquisition (Won et al. 2003). As a result, their growth could be fast enough to possibly avoid being outcompeted and smothered by larger migrants (Nedoncelle et al. 2015). Since Nedoncelle et al. (2014) estimated the mean yearly shell growth rate of *B. azoricus* at ~ 1.68 cm yr^{-1}, it is plausible that medium mussels (~ 3 cm long) could grow to become large mussels (~ 6 cm) within 2–3 yr. Outside venting areas, a net loss of medium mussels favored the colonization of smaller individuals. As mortality and migration create vacant habitats, those can be colonized through the settlement of smaller individuals, emphasizing the importance of recruitment to maintain the mussel population at the carrying capacity of the edifice. Nevertheless, growth and recruitment rates remain to be confirmed experimentally as a recent post-disturbance monitoring at Lucky Strike rather suggested that the growth of *B. azoricus* individuals was slow, with only a partial recovery of new habitats through recruitment over 2 yr of monitoring (Marticorena et al. 2021). While experimentation is needed, our cartography of changes delineated dynamic areas where the deployment of time-lapse cameras could provide a sub-annual image set to better discern the processes acting under natural conditions (e.g., South-East of Eiffel Tower for large mussel colonization).

The disturbance regime can be defined by its area extent, magnitude, frequency, predictability, and turnover rate (Sousa 1984). These characteristics have great implications for community composition because they contribute to habitat heterogeneity and influence individual survival. Over evolutionary time scales, the disturbance regime is a factor of selection to which species adapt to maintain their populations through time; it has thus a strong influence on community resilience (Levin 1992). Overall, because of the absence of large-scale habitat disturbance or mortality from predation, and since *B. azoricus* mussels are well adapted to fine-scale habitat changes, it is not surprising that the mussel population has been maintained at the carrying capacity of the edifice for years (Cuvelier et al. 2011*b*). The Eiffel Tower edifice harbors a larger talus compared to other sites at Lucky Strike, suggesting high maturity (M. Cannat, pers. com.; *see* Hannington et al. 1995 for the definition of maturity). Maturity provides high stability, extent, and complexity of the habitat, which allows, in turn, the sustainable settlement of an extensive mussel population. Given that the Eiffel Tower hosts large and stable communities of the foundation species *B. azoricus*, such mature vent edifices may be keystone features for the regional maintenance of vent populations and biodiversity (e.g., Sarrazin et al. 2020).

Despite Lucky Strike being part of the Azorean marine protected area, our insights enhance our global ecological knowledge on vent ecosystem dynamics at slow-spreading ridges, where seven exploration licenses have been granted so far by the International Seabed Authority (ISA) (i.e., Mid-Atlantic and Indian Ocean Ridges). The observed pluri-decadal stability lines up with other edifice monitoring that depicted decadal stability of vent edifice habitats and associated communities at slow-spreading features (MAR: Cuvelier et al. 2011*b*; Copley et al. 2007; South-West Indian Ridge: Zhou et al. 2018; Pacific back-arc basins: Sen et al. 2014). In addition to the rarity of eruptive events at slow-spreading ridges (i.e., millennia; Rubin et al. 2012), the cumulative evidences indicate the lack of trait selection providing resilience capacity toward disturbance for the vent fauna, being natural or anthropogenic such as deep-sea mining (Du Preez and Fisher 2018). This underlines the need for a precautionary approach to mining activities until more knowledge is gained to define exploitation guidelines (Van Dover et al. 2018).

Microbial mat dynamics

We observed a spectacular decline in microbial mat cover from 2015 to 2020, suggesting that microbial mat dynamics may vary on more rapid time scales than vent megafaunal assemblages. This is supported by the results of Van Audenhaege et al. (2022) who reported periods of absence/presence over only a few months in an area of diffuse outflow at the base of the Eiffel Tower over 7 yr of monitoring. However, this decline detected between 2015 and 2018 contrasts with the general faunal and habitat stability. While biotic factors like grazing activities can strongly regulate microbial cover (Micheli et al. 2002; Cuvelier et al. 2011*a*), microbial mat dynamics may also be sensitive to telluric events, and this may explain that rearrangement at depth of the plumbing system detected in September 2015 coincides with the decline of microbial mat cover detected between 2015 and 2018 (Ballu et al. 2019; this study). As suggested by a switch in the microbial composition of iron-rich mats in 2016 (Astorch-Cardona et al. 2023), the 2015 event could have created temporary conditions also favoring a community change in filamentous mats at Eiffel Tower.

Similarly, the breakpoint detected between 1998 and 2001 coincided with a magmatic episode detected by earthquake swarms in 2001 at Lucky Strike, which was followed by an increase in filamentous mats abundance and a subsequent decline till 2008 (Dziak et al. 2004; this study). At the Eiffel Tower, microbial mats are sustained by distal exposure to plumes of focused vent outflows (Girard et al. 2020). Therefore, despite the apparent stability in venting activity, the overall decline of microbial mat could be explained by particular changes in the vent fluid composition (e.g., chlorine increase as Ballu et al. 2019 detected at the central "Lava Lake" and Eiffel Tower edifice of Lucky Strike). Over time, the recurrence of those observations enabled by the multidisciplinary EMSO-Azores observatory, will likely shed light on the mechanisms and ecological implications of arrhythmic change in microbial mat cover.

Conclusion

This study showed that photogrammetry is a suitable method for multi-scale data acquisition in remote underwater environments to investigate the large-scale maintenance of mosaic communities, which is also the objective of the "patch-dynamics" approach in landscape ecology (Paine and Levin 1981; Levin 1992). Our results emphasized that the predominant scales of variability in faunal distribution and venting activity at the Eiffel Tower restricted to the submeter scale. At large scales, however, the lack of significant shifts in the habitat over two decades explains the overall stability of faunal assemblages. In this study, we observed strong similarities in scales and patterns of environmental and faunal variability in the vicinity of vent exits with those recorded from sub-monthly long-term monitoring at the assemblage scale (Van Audenhaege et al. 2022). This consistency between the two studies shows that the mechanisms and processes observed at a single vent outflow with sub-monthly images could be extrapolated over the edifice over at least two decades. Multi-scale data acquisition, made possible with pluri-disciplinary deep-sea observatories, may thus be particularly useful for disentangling the relevant processes shaping community dynamics at deep-sea hydrothermal vents. Finally, the methodology proposed in this study could be reused to optimize standardization for the spatiotemporal monitoring of complex habitats at slow-spreading centers, particularly in the context of deep-sea mining.

Data availability statement

Data are stored in the SEANOE database: (1) 3D models of 2015 (doi: 10.17882/79218), 2018 (doi: 10.17882/92215) and 2020 (doi: 10.17882/92219) and (2) image annotations for the 2D annotations from 1994 to 2008 (doi: 10.17882/95808) and 3D annotations from 2015 to 2020 and their HTML displays (doi: 10.17882/96475). The R code to compute figures is available in Supporting Information Materials.

References

Arnaubec, A., M. Ferrera, J. Escartín, M. Matabos, N. Gracias, and J. Opderbecke. 2023. Underwater 3D reconstruction from video or still imagery: *Matisse and 3DMetrics* processing and exploitation software. J. Mar. Sci. Eng. **11**: 985. doi:10.3390/jmse11050985

Astorch-Cardona, A., M. Guerre, A. Dolla, V. Chavagnac, and C. Rommevaux. 2023. Spatial comparison and temporal evolution of two marine iron-rich microbial mats from the Lucky Strike Hydrothermal Field, related to environmental variations. Front. Mar. Sci. **10**: 1038192. doi:10.3389/fmars.2023.1038192

Ballu, V., T. Barreyre, M. Cannat, L. Testut, W. Crawford, J. Escartín, T. Coulombier, and V. Chavagnac. 2019. What happened in 2015 at the Lucky Strike volcano? Geophys. Res. Abstr. 21: EGU2019-13294.

Barreyre, T., J. Escartín, R. Garcia, M. Cannat, E. Mittelstaedt, and R. Prados. 2012. Structure, temporal evolution, and heat flux estimates from the Lucky Strike deep-sea hydrothermal field derived from seafloor image mosaics. Geochem. Geophys. **13**: 1–29. doi:10.1029/2011GC003990

Barreyre, T., J. Escartín, R. A. Sohn, M. Cannat, V. Ballu, and W. C. Crawford. 2014. Temporal variability and tidal modulation of hydrothermal exit-fluid temperatures at the Lucky Strike deep-sea vent field, Mid-Atlantic Ridge. J. Geophys. Res.: Solid Earth **119**: 2544–2566. doi:10.1002/2013JB010478

Bertness, M. D., and E. Grosholtz. 1985. Population dynamics of the ribbed mussel, *Geukensia demissa*: The costs and benefits of an aggregated distribution. Oecologia **67**: 192–204. doi:10.1007/BF00384283

Boittiaux, C., C. Dune, M. Ferrera, A. Arnaubec, R. Marxer, M. Matabos, L. van Audenhaege, and V. Hugel. 2023. Eiffel Tower: A deep-sea underwater dataset for long-term visual localization. Int. J. Rob. Res. **42**: 689–699. doi:10.1177/02783649231177322

Borcard, D., F. Gillet, and P. Legendre. 2018. Numerical ecology with R, 2nd ed. Springer International Publishing AG.

Boschen, R. E., A. A. Rowden, M. R. Clark, and J. P. A. Gardner. 2013. Mining of deep-sea seafloor massive sulfides: A review of the deposits, their benthic communities, impacts from mining, regulatory frameworks and management strategies. Ocean Coast. Manag. **84**: 54–67. doi:10.1016/j.ocecoaman.2013.07.005

Cannat, M. 2018. MOMARSAT2018. French Oceanographic Cruises. doi:10.17600/18000514

Cannat, M., and P.-M. Sarradin. 2010. MOMARSAT: Monitoring the Mid-Atlantic Ridge. French Oceanographic Cruises. doi:10.18142/130

Chavagnac, V., T. Leleu, F. Fontaine, M. Cannat, G. Ceuleneer, and A. Castillo. 2018. Spatial variations in vent chemistry at the Lucky Strike hydrothermal field, Mid-Atlantic Ridge (37°N): Updates for subseafloor flow geometry from the

newly discovered Capelinhos vent. Geochem. Geophys. Geosyst. **19**: 4444–4458. doi:10.1029/2018GC007765

Comtet, T., and D. Desbruyères. 1998. Population structure and recruitment in mytilid bivalves from the Lucky Strike and Menez Gwen hydrothermal vent fields (37°17′N and 37°50′N on the Mid-Atlantic Ridge). Ecology **163**: 165–177. doi:10.3354/meps163165

Copley, J. T. P., P. B. K. Jorgensen, and R. A. Sohn. 2007. Assessment of decadal-scale ecological change at a deep Mid-Atlantic hydrothermal vent and reproductive time-series in the shrimp *Rimicaris exoculata*. J. Mar. Biol. Assoc. UK **95**: 859–867. doi:10.1017/S0025315414001738

Crépeau, V., M. A. Cambon Bonavita, F. Lesongeur, H. Randrianalivelo, P. M. Sarradin, J. Sarrazin, and A. Godfroy. 2011. Diversity and function in microbial mats from the Lucky Strike hydrothermal vent field. FEMS Microbiol. Ecol. **76**: 524–540. doi:10.1111/j.1574-6941.2011.01070.x

Cucchiaro, S., M. Cavalli, D. Vericat, S. Crema, M. Llena, A. Beinat, L. Marchi, and F. Cazorzi. 2018. Monitoring topographic changes through 4D-structure-from-motion photogrammetry: Application to a debris-flow channel. Environ. Earth Sci. **77**: 632. doi:10.1007/s12665-018-7817-4

Cuvelier, D., J. Sarrazin, A. Colaço, J. Copley, D. Desbruyères, A. G. Glover, P. Tyler, and R. Serrão Santos. 2009. Distribution and spatial variation of hydrothermal faunal assemblages at Lucky Strike (Mid-Atlantic Ridge) revealed by high-resolution video image analysis. Deep-Sea Res. I: Oceanogr. Res. Pap. **56**: 2026–2040. doi:10.1016/j.dsr.2009.06.006

Cuvelier, D., and others. 2011*a*. Hydrothermal faunal assemblages and habitat characterisation at the Eiffel Tower edifice (Lucky Strike, Mid-Atlantic Ridge). Mar. Ecol. **32**: 243–255. doi:10.1111/j.1439-0485.2010.00431.x

Cuvelier, D., J. Sarrazin, A. Colaço, J. T. Copley, A. G. Glover, P. A. Tyler, R. S. Santos, and D. Desbruyères. 2011*b*. Community dynamics over 14 years at the Eiffel Tower hydrothermal edifice on the Mid-Atlantic Ridge. Limnol. Oceanogr. **56**: 1624–1640. doi:10.4319/lo.2011.56.5.1624

Cuvelier, D., F. de Busserolles, R. Lavaud, E. Floc'h, M. C. Fabri, P. M. Sarradin, and J. Sarrazin. 2012. Biological data extraction from imagery—How far can we go? A case study from the Mid-Atlantic Ridge. Mar. Environ. Res. **82**: 15–27. doi:10.1016/j.marenvres.2012.09.001

Cuvelier, D., P. Legendre, A. Laës-Huon, P. M. Sarradin, and J. Sarrazin. 2017. Biological and environmental rhythms in (dark) deep-sea hydrothermal ecosystems. Biogeosciences **14**: 2955–2977. doi:10.5194/bg-14-2955-2017

Desbruyères, D., M. Segonzac, and M. Bright. 2006. Handbook of deep-sea hydrothermal. Quae.

Du Preez, C., and C. R. Fisher. 2018. Long-term stability of back-arc basin hydrothermal vents. Front. Mar. Sci. **5**: 54. doi:10.3389/fmars.2018.00054

D'Urban Jackson, T., G. J. Williams, G. Walker-Springett, and A. J. Davies. 2020. Three-dimensional digital mapping of ecosystems: A new era in spatial ecology. Proc. R. Soc. B Biol. Sci. **287**: 20192383. doi:10.1098/rspb.2019.2383

Dziak, R. P., D. K. Smith, D. W. R. Bohnenstiehl, C. G. Fox, D. Desbruyères, H. Matsumoto, M. Tolstoy, and D. J. Fornari. 2004. Evidence of a recent magma dike intrusion at the slow spreading Lucky Strike segment, Mid-Atlantic Ridge. J. Geophys. Res.: Solid Earth **109**: 1–15. doi:10.1029/2004JB003141

Gerdes, K., P. M. Arbizu, U. Schwarz-Schampera, M. Schwentner, and T. C. Kihara. 2019. Detailed mapping of hydrothermal vent fauna: A 3D reconstruction approach based on video imagery. Front. Mar. Sci. **6**: 96. doi:10.3389/fmars.2019.00096

Girard, F., J. Sarrazin, A. Arnaubec, M. Cannat, P.-M. Sarradin, B. Wheeler, and M. Matabos. 2020. Currents and topography drive assemblage distribution on an active hydrothermal edifice. Prog. Oceanogr. **187**: 102397. doi:10.1016/j.pocean.2020.102397

Hannington, M. D., I. Jonasson, P. M. Herzig, and S. Petersen. 1995. Physical and chemical processes of seafloor mineralization at mid-ocean ridges, p. 115–157. *In* S. E. Humphris, R. A. Zierenberg, L. S. Mullineaux, and R. E. Thomson [eds.], Seafloor hydrothermal systems: Physical, chemical, biological, and geological interactions. American Geophysical Union. doi:10.1029/GM091p0115

Henry, M. S., J. J. Childress, and D. Figueroa. 2008. Metabolic rates and thermal tolerances of chemoautotrophic symbioses from Lau Basin hydrothermal vents and their implications for species distributions. Deep-Sea Res. I: Oceanogr. Res. Pap. **55**: 679–695. doi:10.1016/j.dsr.2008.02.001

Horn, H. S. 1976. Succession, p. 187–204. *In* R. M. May [ed.], Theoretical ecology. Principles and applications. WB Saunders.

Humphris, S. E., D. J. Fornari, D. S. Scheirer, C. R. German, and L. M. Parson. 2002. Geotectonic setting of hydrothermal activity on the summit of Lucky Strike Seamount (37°17′N, Mid-Atlantic Ridge). Geochem. Geophys. Geosyst. **3**: 1–24. doi:10.1029/2001GC000284

Husson, B., P.-M. Sarradin, D. Zeppilli, and J. Sarrazin. 2017. Picturing thermal niches and biomass of hydrothermal vent species. Deep-Sea Res. II: Top. Stud. Oceanogr. **137**: 6–25. doi:10.1016/j.dsr2.2016.05.028

Jannasch, H. W. 1985. The chemosynthetic support of life and the microbial diversity at deep-sea hydrothermal vents. Proc. R. Soc. London. Ser. B. Biol. Sci. **225**: 277–297. doi:10.1098/rspb.1985.0062

Johnson, K. S., J. J. Childress, C. L. Beehler, and C. M. Sakamoto. 1994. Biogeochemistry of hydrothermal vent mussel communities: The deep-sea analogue to the intertidal zone. Deep-Sea Res. I: Oceanogr. Res. Pap. **41**: 993–1011. doi:10.1016/0967-0637(94)90015-9

Kwasnitschka, T., T. H. Hansteen, C. W. Devey, and S. Kutterolf. 2013. Doing fieldwork on the seafloor: Photogrammetric techniques to yield 3D visual models from

ROV video. Comput. Geosci. **52**: 218–226. doi:10.1016/j.cageo.2012.10.008

Lee, R. W., K. Robert, M. Matabos, A. E. Bates, and S. K. Juniper. 2015. Temporal and spatial variation in temperature experienced by macrofauna at Main Endeavour hydrothermal vent field. Deep-Sea Res. I: Oceanogr. Res. Pap. **106**: 154–166. doi:10.1016/j.dsr.2015.10.004

Lenihan, H. S., S. W. Mills, L. S. Mullineaux, C. H. Peterson, C. R. Fisher, and F. Micheli. 2008. Biotic interactions at hydrothermal vents: Recruitment inhibition by the mussel *Bathymodiolus thermophilus*. Deep-Sea Res. I: Oceanogr. Res. Pap. **55**: 1707–1717. doi:10.1016/j.dsr.2008.07.007

Levin, S. A. 1992. The problem of pattern and scale in ecology. Ecology **73**: 1943–1967. doi:10.2307/1941447

Marticorena, J., and others. 2021. Recovery of hydrothermal vent communities in response to an induced disturbance at the Lucky Strike vent field (Mid-Atlantic Ridge). Mar. Environ. Res. **168**: 105316. doi:10.1016/j.marenvres.2021.105316

Mat, A., and others. 2020. Biological rhythms in the deep-sea hydrothermal mussel *Bathymodiolus azoricus*. Nat. Commun. **11**: 3454. doi:10.1038/s41467-020-17284-4

Matabos, M., and others. 2015. Behavioural study of two hydrothermal crustacean decapods: *Mirocaris fortunata* and *Segonzacia mesatlantica*, from the Lucky Strike vent field (Mid-Atlantic Ridge). Deep-Sea Res. II: Top. Stud. Oceanogr. **121**: 146–158. doi:10.1016/j.dsr2.2015.04.008

Matabos, M., and others. 2022. Integrating multidisciplinary observations in vent environments (IMOVE): Decadal progress in deep-sea observatories at hydrothermal vents. Front. Mar. Sci. **9**: 866422. doi:10.3389/fmars.2022.866422

Micheli, F., C. H. Peterson, L. S. Mullineaux, C. R. Fisher, S. W. Mills, G. Sancho, G. A. Johnson, and H. S. Lenihan. 2002. Predation structures communities at deep-sea hydrothermal vents. Ecol. Monogr. **72**: 365–382. doi:10.1890/0012-9615(2002)072[0365:PSCADS]2.0.CO;2

Moulon, P., P. Monasse, R. Perrot, and R. Marlet. 2017. OpenMVG: Open multiple view geometry, p. 60–74. *In* B. Kerautret, M. Colom, and P. Monasse [eds.], Reproducible research in pattern recognition, v. **10214**. Springer. doi:10.1007/978-3-319-56414-2_5

Mullineaux, L. S., C. H. Peterson, F. Micheli, and S. W. Mills. 2003. Successional mechanism varies along a gradient in hydrothermal fluid flux at deep-sea vents. Ecol. Monogr **73**: 523–542. doi:10.1890/02-0674

Nedoncelle, K., N. Le Bris, M. de Rafélis, N. Labourdette, and F. Lartaud. 2014. Non-equilibrium fractionation of stable carbon isotopes in chemosynthetic mussels. Chem. Geol. **387**: 35–46. doi:10.1016/j.chemgeo.2014.08.002

Nedoncelle, K., F. Lartaud, L. Contreira Pereira, M. Yücel, A. M. Thurnherr, L. Mullineaux, and N. Le Bris. 2015. *Bathymodiolus* growth dynamics in relation to environmental fluctuations in vent habitats. Deep-Sea Res. I: Oceanogr. Res. Pap. **106**: 183–193. doi:10.1016/j.dsr.2015.10.003

Ondréas, H., M. Cannat, Y. Fouquet, A. Normand, P. M. Sarradin, and J. Sarrazin. 2009. Recent volcanic events and the distribution of hydrothermal venting at the Lucky Strike hydrothermal field, Mid-Atlantic Ridge. Geochem. Geophys. Geosyst. **10**: 1–18. doi:10.1029/2008GC002171

Paine, R. T., and S. A. Levin. 1981. Intertidal landscapes: Disturbance and the dynamics of pattern. Ecol. Monogr. **51**: 145–178. doi:10.2307/2937261

Podowski, E. L., T. S. Moore, K. A. Zelnio, G. W. Luther, and C. R. Fisher. 2009. Distribution of diffuse flow megafauna in two sites on the Eastern Lau Spreading Center, Tonga. Deep-Sea Res. I: Oceanogr. Res. Pap. **56**: 2041–2056. doi:10.1016/j.dsr.2009.07.002

Pulido Mantas, T., and others. 2023. Photogrammetry, from the land to the sea and beyond: A unifying approach to study terrestrial and marine environments. J. Mar. Sci. Eng. **11**: 759. doi:10.3390/jmse11040759

Robert, K., D. O. B. Jones, A. Georgiopoulou, and V. A. I. Huvenne. 2020. Cold-water coral assemblages on vertical walls from the Northeast Atlantic. Divers. Distrib. **26**: 284–298. doi:10.1111/ddi.13011

Rubin, K. H., and others. 2012. Volcanic eruptions in the deep sea. Oceanography **25**: 142–147. doi:10.5670/oceanog.2012.12

Sarradin, P.-M., and M. Cannat. 2015. MOMARSAT2015. French Oceanographic Cruises. doi:10.17600/15000200

Sarradin, P.-M., and J. Legrand. 2020. MOMARSAT2020. French Oceanographic Cruises. doi:10.17600/18000684

Sarrazin, J., and K. S. Juniper. 1998. The use of video imagery to gather biological information at deep-sea hydrothermal vents. Cah. Biol. Mar. **39**: 255–258.

Sarrazin, J., V. Robigou, S. K. Juniper, and J. R. Delaney. 1997. Biological and geological dynamics over four years on a high-temperature sulfide structure at the Juan de Fuca Ridge hydrothermal observatory. Mar. Ecol. Prog. Ser. **153**: 5–24. doi:10.3354/meps153005

Sarrazin, J., C. Levesque, S. K. Juniper, and M. K. Tivey. 2002. Mosaic community dynamics on Juan de Fuca Ridge sulphide edifices: Substratum, temperature and implications for trophic structure. Cah. Biol. Mar. **43**: 275–279. doi:10.21411/cbm.a.8e98c7cc

Sarrazin, J., M. Portail, E. Legrand, C. Cathalot, A. Laes, N. Lahaye, P. M. Sarradin, and B. Husson. 2020. Endogenous versus exogenous factors: What matters for vent mussel communities? Deep-Sea Res. I: Oceanogr. Res. Pap. **160**: 103260. doi:10.1016/j.dsr.2020.103260

Sarrazin, J., C. Cathalot, A. Laes, J. Marticorena, L. Michel, and M. Matabos. 2022. Integrated study of new faunal assemblages dominated by gastropods at three vent fields along the Mid-Atlantic Ridge: Diversity, structure, composition and trophic interactions. Front. Mar. Sci. **9**: 925419. doi:10.3389/fmars.2022.925419

Sen, A., and others. 2014. Community succession in hydrothermal vent habitats of the Eastern Lau Spreading Center

and Valu Fa Ridge, Tonga. Limnol. Oceanogr. **59**: 1510–1528. doi:10.4319/lo.2014.59.5.1510

Shank, T. M., D. J. Fornari, K. L. Von Damm, M. D. Lilley, R. M. Haymon, and R. A. Lutz. 1998. Temporal and spatial patterns of biological community development at nascent deep-sea hydrothermal vents (9°50′N, East Pacific Rise). Deep-Sea Res. II: Top. Stud. Oceanogr. **45**: 465–515. doi:10.1016/S0967-0645(97)00089-1

Sousa, W. P. 1984. The role of disturbance in natural communities. Annu. Rev. Ecol. Syst. **15**: 353–391. doi:10.1146/annurev.es.15.110184.002033

Tunnicliffe, V. 1991. The biology of hydrothermal vents: Ecology and evolution, p. 319–407. *In* H. Barnes, M. Barnes, A. D. Ansell, and R. N. Gibson [eds.], Oceanography and marine biology annual review. Aberdeen Univ. Press.

Tunnicliffe, V., and S. K. Juniper. 1990. Dynamic character of the hydrothermal vent habitat and the nature of sulphide chimney fauna. Progr. Oceanogr. **24**: 1–13. doi:10.1016/0079-6611(90)90015-T

Van Audenhaege, L., M. Matabos, A. Brind'Amour, J. Drugmand, A. Laës-Huon, P.-M. Sarradin, and J. Sarrazin. 2022. Long-term monitoring reveals unprecedented stability of a vent mussel assemblage on the Mid-Atlantic Ridge. Prog. Oceanogr. **204**: 102791. doi:10.1016/j.pocean.2022.102791

Van Dover, C. L. 2014. Impacts of anthropogenic disturbances at deep-sea hydrothermal vent ecosystems: A review. Mar. Environ. Res. **102**: 59–72. doi:10.1016/j.marenvres.2014.03.008

Van Dover, C. L., and others. 2018. Scientific rationale and international obligations for protection of active hydrothermal vent ecosystems from deep-sea mining. Mar. Policy **90**: 20–28. doi:10.1016/j.marpol.2018.01.020

Won, Y. J., S. J. Hallam, G. D. O'Mullan, I. L. Pan, K. R. Buck, and R. C. Vrijenhoek. 2003. Environmental acquisition of thiotrophic endosymbionts by deep-sea mussels of the genus *Bathymodiolus*. Appl. Environ. Microbiol. **69**: 6785–6792. doi:10.1128/AEM.69.11.6785-6792.279003

Zhou, Y., and others. 2018. Characterization of vent fauna at three hydrothermal vent fields on the Southwest Indian Ridge: Implications for biogeography and interannual dynamics on ultraslow-spreading ridges. Deep-Sea Res. I: Oceanogr. Res. Pap. **137**: 1–12. doi:10.1016/j.dsr.2018.05.001

Acknowledgment

We firstly thank the crew of the R/Vs *Pourquoi pas?* and *L'Atalante* as well as the pilots of the ROV *Victor6000* during the MoMARSAT cruises of 2015, 2018, and 2020. We are grateful to M. Ferreira, C. Boittiaux, and more generally, the PRAO research labs of Ifremer DFO department, for the development of high-resolution optical sensors of the ROV as well as reconstruction of 3D models. We are grateful to D. Cuvelier, who provided annotations from 1998 to 2008. We would like to thank F. Girard for sharing her expertise on the annotation of the 2015 3D model. We express our gratitude to the editor, associated editor and two anonymous reviewers, who significantly improved the manuscript with their suggestions. This manuscript was professionally edited by C. Engel-Gautier. This work and LVA's PhD thesis were supported by the European Union's Horizon 2020 research and innovation project iAtlantic under Grant Agreement No. 818123. This output reflects only the authors' view and the European Union cannot be held responsible for any use that may be made of the information contained therein. We also acknowledge the financial support from the EU project EMSO (http://www.emso-eu.org/) and the French observatory EMSO-Azores funded by Ifremer and CNRS.

Conflict of Interest

None declared.

Submitted 20 February 2023
Revised 19 September 2023
Accepted 12 December 2023

Associate editor: Birte Matthiessen